Observation of Magnetically-Induced atomic transitions of the ^{133}Cs 6s $^2S_{1/2} \rightarrow$ 7p $^2P_{3/2}$ line at 456 nm

Armen Sargsyan[a], Arevik Amiryan[b], Emmanuel Klinger[b,*], David Sarkisyan[a]

[a] *Institute for Physical Research – National Academy of Sciences of Armenia, Ashtarak-2 0203, Armenia*
[b] *Université Marie et Louis Pasteur, Supmicrotech, CNRS, Institut FEMTO-ST, F-25000 Besançon, France*

Abstract

It has recently been demonstrated that magnetically induced (MI) transitions, a class of transitions forbidden at zero magnetic field, of the ^{133}Cs 6s $^2S_{1/2} \rightarrow$ 6p $^2P_{3/2}$ (D_2) line, exhibit promising features for high-resolution physics applications in the near-infrared range. In this work, we study a group of seven MI transitions ($F_g = 3 \rightarrow F_e = 5$) of the ^{133}Cs 6s $^2S_{1/2} \rightarrow$ 7p $^2P_{3/2}$ line at $\lambda = 456$ nm. The experimental measurements are in very good agreement with theoretical predictions based on the diagonalization of the Zeeman Hamiltonian. In magnetic fields ranging from $0.2 - 3.4$ kG, these transitions reach a maximum intensity above that of conventional transitions. Another noteworthy property is their large frequency shift, reaching approximately 17 GHz with respect to the unperturbed hyperfine transitions in magnetic fields of about 3 kG. These interesting properties may prove useful for the realization of optical frequency references or magnetometers with sub-micron spatial resolution in the blue region of the spectrum.

Keywords: Sub-Doppler spectroscopy, Magnetically-induced transitions, Alkali atoms, Nanometric-thin cells

*Corresponding author
Email address: emmanuel.klinger@femto-st.fr (Emmanuel Klinger)

1. Introduction

Magneto-optical processes are widely used in many areas as they encompass a large range of applications, such as optical magnetometry [1], narrow-band atomic filtering [2], tunable laser frequency locking [3], etc. For this reason, the interaction of light with an atomic vapor perturbed by a magnetic field has been widely studied and is still a topic of interest [4–7]. Recently, attention has been focused on atomic transitions between ground and excited hyperfine levels satisfying an apparent $F_e - F_g = \Delta F = \pm 2$ selection rule [8–12]. The intensity of these transitions is zero when no external magnetic field is applied but significantly increases with the magnetic field amplitude. These transitions are referred to as magnetically induced (MI) transitions. They arise from the mixing of levels induced by the magnetic field. Indeed, the external magnetic field couples magnetic sublevels with $\Delta m_F = 0$, for which the matrix elements are nonzero only when $\Delta F = \pm 1$ [4]. Transition obeying $\Delta F = \pm 2$ then become allowed when the corresponding m_F sublevel are "mixed" through a common sublevel.

Important peculiarities have been demonstrated for the group of seven $F = 3 \rightarrow 5'$ (where the prime indicates the excited state) MI transitions of the 6s $^2S_{1/2} \rightarrow$ 6p $^2P_{3/2}$ ^{133}Cs atoms ($I = 7/2$) [13]. The intensities of MI transitions with $\Delta F = +2$ are maximal (and the number of MI transitions is also maximal) for σ^+ circularly polarized laser radiation, whereas the intensities of MI transitions with $\Delta F = -2$ are minimal (and the number of MI transitions is also minimal) for σ^- circularly polarized radiation, see Fig. 1. Note that in this case, only one transition remains and that its intensity is by several times weaker than the strongest MI transition in the case of for σ^+ excitation. This demonstrates a remarkable difference in the behavior of the $F = 3 \rightarrow 5'$ transitions depending on the use of right- or left-handed circularly-polarized radiation.

An attractive feature of these MI transitions is their large frequency shift with respect to the unperturbed hyperfine transitions in a magnetic field, which reaches approximately 17 GHz at a magnetic field of $B \approx 3$ kG. Moreover, it is important to note that these transitions are formed on the high-frequency wing of the spectrum and do not overlap with other transitions, which is of practical interest. For example, magnetically induced transitions of the ^{133}Cs D_2 line have been successfully used for the realization of electromagnetically induced transparency [14].

In this article, we report on a combined experimental and theoretical

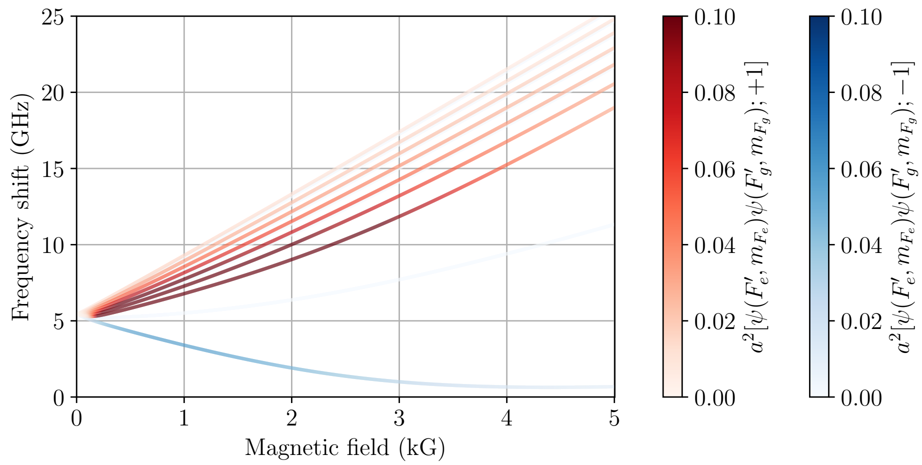

Figure 1: Evolution of $F = 3 \to 5'$ MI transitions of the ^{133}Cs D_2 line in a magnetic field. The plot shows the evolution of the transition frequency as a function of the magnetic field amplitude. Here, the zero frequency corresponds to the weighted center of the D_2 line, i.e. $\nu_{D_2} \approx 351.725719$ THz. The line colors reflect the evolution of the transition intensity, through the transfer coefficient $a^2[\psi(F'_e, m_{F_e})\psi(F'_g, m_{F_g}); q]$ in the case of σ^+ ($q = +1$, red) and σ^- ($q = -1$, blue) optical polarization of the resonant light. The theoretical model used to calculate the behavior of atomic transitions in an external static magnetic is based on constructing the magnetic Hamiltonian [4], including the entire hyperfine manifold in the $|F, m_F\rangle$ basis, and then perform numerical diagonalization, see Sec. 2.

study of $F = 3 \to 5'$ MI transitions of the 6s $^2S_{1/2} \to$ 7p $^2P_{3/2}$ line at 456 nm. This is, to the best of our knowledge, the first time these transitions are studied. Indeed, performing such a study is quite a challenge for the following reasons. (*i*) The frequency spacing between the upper levels of 7p $^2P_{3/2}$ is approximately 3 times smaller than that of the 6p $^2P_{3/2}$ of the D_2 line, $\lambda = 852$ nm [15]. (*ii*) The Doppler width for the 6s $^2S_{1/2} \to$ 7p $^2P_{3/2}$ transition ($\Gamma_D/2\pi = 0.87$ GHz at 180 °C) is approximately 2.5 times larger than that for the D_2 line, which greatly complicates the study of individual atomic transitions, especially in the presence of a magnetic field. (*iii*) The oscillator strength is almost two orders of magnitude smaller here than for the transition to the 6p $^2P_{3/2}$ state [16, 17]. For these reasons, spectroscopic studies of the 6s $^2S_{1/2} \to$ 7p $^2P_{3/2}$ transition are scarce in the literature. Previous studies have focused on the observation of these transitions in nano- [18, 19] and millimeter-sized [20] vapor cells and their application for laser frequency stabilization [21, 22]. To study a large number closely-spaced atomic transitions split by a magnetic fields, a sub-Doppler technique is thus required.

As was previously shown, using nanocell combined with derivative spectroscopy allows one to study individual atomic transitions even in the presence of a large number of Zeeman components [10]. To spectrally separate MI transitions from other atomic transitions that form in the spectrum in a magnetic field, we used a process referred to as selective reflection (SR). The SR of laser radiation is formed at the boundary between an alkali metal vapor and dielectric windows and is known to provide nearly Doppler-free spectral resolution, see e.g. Refs. [23–25], usually employed to study atom-surface interactions [26, 27] or spectral features in high density vapor cells [28, 29].

The manuscript is organized as follows. In Sec. 2, we briefly review how to compute the evolution of transition frequencies and intensities in a magnetic field and show the prediction for the 6s $^2\mathrm{S}_{1/2} \rightarrow$ 7p $^2\mathrm{P}_{3/2}$ transition. Sec. 3 is dedicated to detailing the experimental setup. Finally, in Sec. 4 we compare experimental and theoretical results.

2. Theoretical considerations

To calculate the evolution of alkali transitions in an external magnetic field, we follow the procedure detailed in Ref. [4]. Briefly, this consists in diagonalizing the Hamiltonian matrix which accounts for the hyperfine atomic structure and the Zeeman Hamiltonian

$$H = H_{\mathrm{hfs}} + \frac{\mu_B}{\hbar}(g_S\, S_z + g_L\, L_z + g_I\, I_z)B_z\,, \qquad (1)$$

where μ_B is the Bohr magneton [30], $g_{S,L,I}$ are the Landé factors [31] and S_z, L_z, I_z the projection of quantum numbers on the z-axis (quantization axis). Expressions for diagonal and non-diagonal matrix elements in the base $|F, m_F\rangle$ are given in Ref. [4]. Diagonalizing this matrix provides access, on the one hand, to the eigenvalues directly linked to the resonance frequencies. On the other hand, the transition intensities are proportional to the squared dipole moment, given, in the coupled basis $|F, m_F\rangle$, by

$$|\langle e\|d\|g\rangle|^2 = \frac{3\epsilon_0\hbar\lambda_{eg}^3}{8\pi^2}\cdot\Gamma_{\mathrm{N}}\, a^2[\psi(F_e', m_{F_e}); \psi(F_g', m_{F_g}); q]\,, \qquad (2)$$

where $\Gamma_{\mathrm{N}}/2\pi \approx 1.16\,\mathrm{MHz}$ [17] and λ_{eg} are respectively the natural linewidth and the wavelength of the 6s $^2\mathrm{S}_{1/2} \rightarrow$ 7p $^2\mathrm{P}_{3/2}$ transition. The transfer coefficients $a[\psi(F'_e, m_{F_e}); \psi(F'_g, m_{F_g}); q]$ modified by the field are calculated using the eigenvectors. Here, $q = 0, \pm 1$ is associated with the polarization of the incident laser field. This computation is repeated for every value of the magnetic field to construct the evolution of the transitions. Note that, in the case of the alkali D lines, these can be computed with *ElecSus* [32].

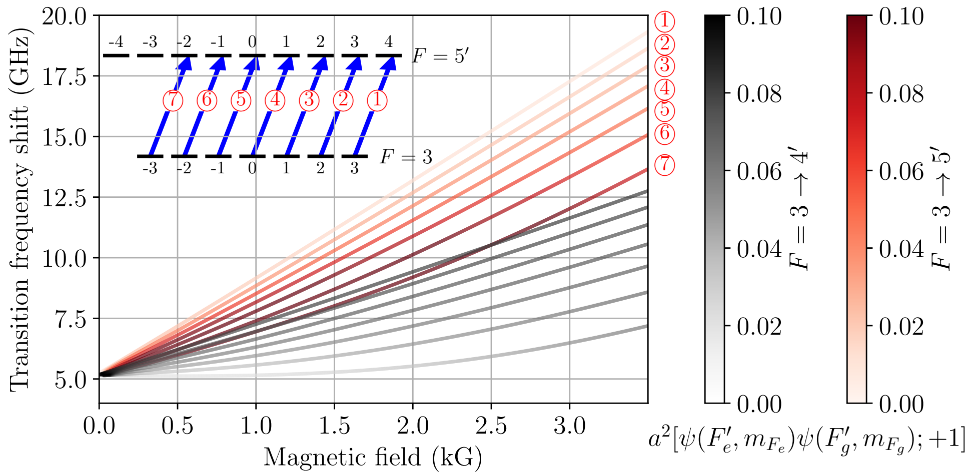

Figure 2: Evolution of $F = 3 \to 5'$ MI transitions (red) and $F = 3 \to 4'$ (black) of the ^{133}Cs 6s ^{2}S$_{1/2} \to$ 7p ^{2}P$_{3/2}$ line in a magnetic field. The plot shows the evolution of the transition frequency as a function of the magnetic field intensity. Here, the zero frequency corresponds to the weighted center of the D$_2$ line, i.e. $\nu_{6S_{1/2}\to 7P_{3/2}} \approx 657.936362$ THz [15]. The line colors reflect the evolution of the transition intensity, through the transfer coefficient $a^2[\psi(F'_e, m_{F_e})\psi(F'_g, m_{F_g}); q]$, in the case of σ^+ optically-polarized resonant light ($q = +1$). The inset shows a diagram of the transitions with the corresponding labeling.

In Fig. 2, we plot both the dependence of the frequency and intensity of the $F = 3 \to 5'$ group of transitions under σ^+ laser excitation as a function of the external magnetic field B. This group contains seven magnetic field-induced atomic transitions labeled ① to ⑦, see the inset in Fig. 2. The plot also includes the group of $F = 3 \to 4'$ transitions as these two groups partially overlap at low and intermediate magnetic fields. A comparison of the transition probabilities of 6s ^{2}S$_{1/2} \to$ 6p ^{2}P$_{3/2}$ $F = 3 \to 5'$ and $F = 3 \to 4'$ transitions is shown in the Figure 7 of Ref. [33]. A similar dependence is also observed here in the case of the 6s ^{2}S$_{1/2} \to$ 7p ^{2}P$_{3/2}$ manifold but for another magnetic fields. To qualify these regimes, it is often convenient to introduce the characteristic quantity

$$B_0 = \frac{A_{\mathrm{HFS}}}{\mu_B} \approx 1.6 \text{ kG},$$

where A_{HFS} is the hyperfine structure coupling coefficient for the ^{133}Cs ground level 6s $^2\mathrm{S}_{1/2}$. This quantity describe how strong the interaction of the atoms with the magnetic field is: when $B \ll B_0$, the field is described as low. Conversely, when $B \gg B_0$ the field is described as high and, in between, the field is qualified as intermediate.

In the range of 0.1–3.4 kG, MI transitions are the strongest atomic transitions among all transitions originating from the $F_g = 3$ ground state. Note that the highest intensity corresponds to the MI transition for which the magnetic sublevel of the ground state m_F is minimal ($m_F = -3 \rightarrow -2'$); in this case ⑦. Conversely, the smallest intensity corresponds to transition ①, for which the value of m_F is the largest ($m_F = 3 \rightarrow 4'$). For $B \gg B_0$, our calculations show that the intensity of these MI transitions tends to zero. In addition, for magnetic fields $B > 3$ kG these transitions are formed on the high-frequency wing of the spectrum and do not overlap with others. This behavior is due to the fact that the frequency slope of the $F = 3 \rightarrow 5'$ MI transitions for $B > 2$ kG is approximately 4 MHz/G, while for $F = 3 \rightarrow 4'$ transitions, the frequency slope is approximately 2 MHz/G.

Note that there also exist five MI transitions of the group $F = 2 \rightarrow 4'$ (not shown in Fig. 2), as they are only excited with σ^- circularly-polarized laser radiation. However, these transitions have intensities much weaker than the intensities of the $F = 3 \rightarrow 5'$ group as in the case of the D_2 line [14]. Additionally, there exists a set of MI transitions of the type

$$|F_g = F,\, m_F = 0\rangle \rightarrow |F_e = F,\, m'_F = 0\rangle$$

which are forbidden in zero magnetic field, but can be excited with linearly π-polarized laser excitation when $B > 0$ [34]. It is interesting to note that for $B \gg B_0$, these MI transitions tend toward an asymptotic value. Indeed, at such fields, the coupling between $\mathbf{J}$ and $\mathbf{I}$ break and the splitting of levels is determined by projections m_J and m_I [13]. As a result, atomic levels with $F = 5'$ no longer exists. In summary, our simulations show a total of 17 MI transitions for the $6^2\mathrm{S}_{1/2} \rightarrow 7^2\mathrm{P}_{3/2}$ transition, which expand the possibilities for using magneto-optical processes in the blue spectral region. For the experimental study, we will focus only on the $F = 3 \rightarrow 5'$ MI transitions.

3. Experimental Setup

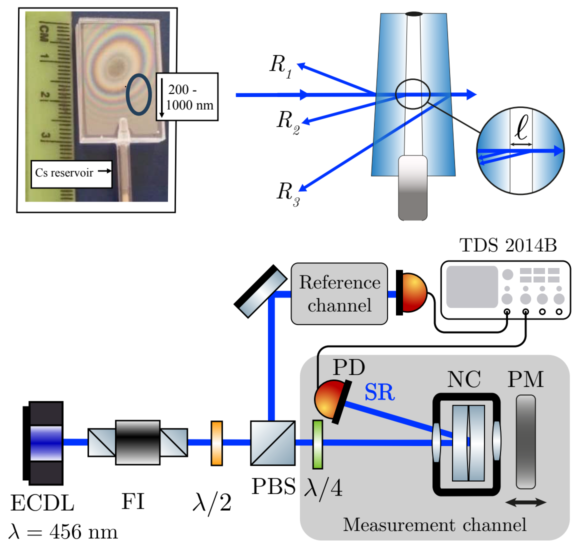

Figure 3: Sketch of the experimental setup. ECDL – extended cavity diode laser operating at 456 nm, FI – Faraday isolator, PBS – polarizing beam splitter, PM – permanent magnet, NC – nanometric-thin cell filled with ^{133}Cs in the oven, PD – photodiodes, TDS 2014B – Digital oscilloscope, $\lambda/2$, $\lambda/4$– half and quarter wave plates. The PM is oriented such that the applied magnetic field $\mathbf{B}$ is collinear with the propagation axis (z-axis) of the laser radiation ($\mathbf{B}\|\mathbf{k}$) in order to excite σ^+ transitions. A part of the laser radiation was directed to an auxiliary unit to provide a frequency reference based on saturated absorption. Upper left inset, is the photograph of the NC; the oval marks 200–1000 nm region of the ^{133}Cs vapor column. Upper right inset, geometry of the three reflected beams. The SR beam propagates in the direction of R_2 and was used to realize sub-Doppler spectroscopy.

In order to resolve Doppler-broadened, closely-spaced, atomic transitions we use selective reflection from a nanocell (NC) combined with derivative spectroscopy. The main advantages of SR from a NC are the following: (i) simplicity of the realization (single beam, as opposed to counter-propagating beams required for e.g. saturated absorption); (ii) absence of crossover (CO) resonances, which is particularly important when studying atomic transitions in an external field as CO resonances split into many additional components; (iii) the amplitudes of the derivatives of SR from a NC are proportional to the probabilities of the atomic transitions.

The sketch of the experimental setup is presented in Fig. 3. We use an external-cavity diode laser (ECDL) with a spectral linewidth of 400 kHz tunable around $\lambda = 456$ nm and resonant with the $6^2S_{1/2} \rightarrow 7^2P_{3/2}$ transition of ^{133}Cs. To avoid feedback in the laser cavity, a Faraday insulator (FI) was used. The incident laser beam is then directed at normal incidence onto the nanocell windows. A photography of the NC (front view) is shown on the left inset of Fig. 3 where we have circled the 200-1000 nm range of thicknesses. The NC consists of ∼2 mm-thick windows made of technical sapphire (Al_2O_3) and a vertical side arm (a sapphire tube reservoir filled with ^{133}Cs metal). The laser beam configuration for SR spectroscopy with the NC is depicted in right inset of Fig. 3. Note that the wedge of the nanocell windows are exaggerated on this diagram. To record the signal of interest (R_2), arising from reflections of the window-vapor and vapor-window interfaces inside the cell, the reflected beam is detected with a photodiode whose signal is fed to a four-channel oscilloscope (Tektronix TDS2014B).

A part of the laser radiation was directed to an auxiliary unit to provide a frequency reference based on saturated absorption [35]. To study MI transitions, a strong permanent neodymium magnet (PM) was mounted on a micrometric-step translation stage in the proximity of the cell's rear window. The B-field strength was varied by simple longitudinal displacement of the magnet. In this configuration, the magnetic field is directed along the laser radiation propagation axis (z, the quantization axis) such that $\mathbf{B} \parallel \mathbf{k}$. The applied B-field was calibrated with a Teslameter HT201 magnetometer.

To overcome smaller signals due to the weaker dipole moments (with respect to the D_2 line), we heat the NC to a temperature of about 180 °C while the windows were maintained at a temperature that was about 20 °C higher to avoid condensation of the atomic vapor on the windows. The laser is shined on the region $\ell \approx 800$ nm. This is chosen for the following reasons: (i) it is close to an odd multiple of $\lambda/4$ (here about 7/4) yielding sub-Doppler features centered on the atomic transition with derivative spectroscopy [24, 36]; *(ii)* it is large enough such that the observed spectra are free from distortion originating from atom-surface interactions [37]; (iii) it allows for a larger signal-to-noise (with respect to smaller thicknesses). The laser power was set to about 30 mW (beam diameter of ≈ 1 mm). Despite this power being high, it was shown to not be saturating in the case of the ^{133}Cs D_2 line recorded with a NC [38].

4. Selective reflection spectra in an external magnetic field

To validate the theoretical model, we have recorded and analyzed experimental SR spectra from a NC obtained for magnetic field in a range of 450 to 800 G. The results are summarized in Fig. 4, were we plot the extracted positions of the $F = 3 \rightarrow 5'$ MI transitions as a function of the applied magnetic field. The recorded positions of these transitions are seen to agree with the predictions following the model described in Sec. 2. Note that for $B > 650$ G, the mode-hop free frequency scanning range of the laser greatly deteriorated at the time the data was acquired for these fields. For this reason, we were not able to record all the seven $F = 3 \rightarrow 5'$ MI transitions.

The top inset in Fig. 4 shows an experimental SR spectrum (blue dots) processed with first order derivative (dSR) and obtained for $B \approx 500$ G. The orange solid line shows the equivalent theoretical spectrum obtained with $\ell = 750$ nm and $B = 500$ G. Details on how to calculate dSR spectrum can be found e.g. in Refs. [18, 25]. Note that, for fields below 2.5 kG, $F = 3 \rightarrow 5'$ MI transitions partially overlap with the group of transitions $F = 3 \rightarrow 4'$ for which one transition can be observed between ⑦ and ⑥ (another one completely overlaps with ⑥ for this magnetic field).

Conclusion

In conclusion, we have studied, both experimentally and theoretically, the magnetic dependence of the high frequency wing spectrum of the 6s $^2S_{1/2} \rightarrow$ 7p $^2P_{3/2}$ transition observed under right-hand circularly-polarized laser light at 456 nm. Our studies have focused on seven $F = 3 \rightarrow 5'$ magnetically-induced transitions. Among the important features of these MI transitions is their large frequency shift with respect to the unperturbed hyperfine transitions, which reaches ~ 17 GHz in magnetic fields of ~ 3 kG, easily achievable with permanent magnets [39]. Besides, they reach their maximum intensity in the magnetic field range of 0.2–3.4 kG where they are more intense than many conventional ($\Delta F = 0, \pm 1$) atomic transitions.

These results are important for both fundamental studies and practical applications, particularly for the development of magnetometers with submicron spatial resolution in the blue spectral region. For example, these seven MI transitions may be used to form EIT in a three-level Ladder system and single out different excitation paths to the 32S Rydberg state of ^{133}Cs atoms with 456 and 1070 nm lasers [40]. Besides, as demonstrated in Ref. [9], using

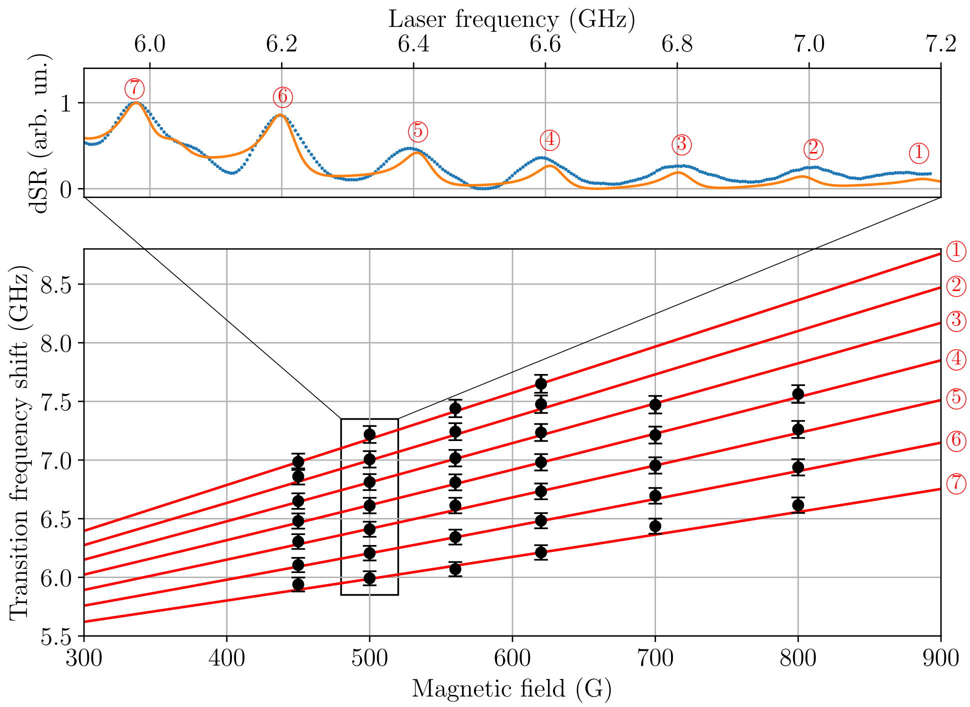

Figure 4: Magnetic dependence of the 6s $^2S_{1/2} \rightarrow$ 7p $^2P_{3/2}$ $F = 3 \rightarrow 5'$ MI transitions labeled ① to ⑦. The dots correspond to the experimental values extracted from the spectrum and the error bars correspond to the each observed transition linewidth. The red solid line correspond to the expected theoretical evolution following the model described in Sec. 2. The top inset shows an example of experimental derivative of selective reflection spectrum (blue dots) recorded for $B \approx 500$ G together with the equivalent theoretical spectrum calculated for $\ell = 750$ nm (orange solid line), see the text.

a nanocell with a thickness $\ell = 100$ nm and $F = 1 \rightarrow 3'$ MI transitions of ^{87}Rb D_2 line, it is possible to realize a magnetometer with a spatial resolution of 1 μm. This is particularly important for mapping magnetic fields with strong spatial gradients exceeding $3\,\mathrm{G}/\mu\mathrm{m}$ [41]. Finally, these transitions may be used to create an optical frequency reference operating at controllable and highly shifted frequencies (with respect to that of the unperturbed hyperfine transition) in the ~ 450 nm blue spectral region.

Author Contributions

Armen Sargsyan: Writing – review & editing, Writing – original draft, Investigation, Funding acquisition, Data curation.

Arevik Amiryan: Writing – review & editing, Writing – original draft, Visualization, Software, Formal analysis.

Emmanuel Klinger: Writing – review & editing, Writing – original draft, Visualization, Software, Formal analysis.

David Sarkisyan: Writing – review & editing, Writing – original draft, Supervision, Investigation, Funding acquisition.

Funding

AS and DS acknowledge financial support from the Higher Education and Science Committee of the MESCS RA under the project No 25RG-1C008.

Declaration of Competing Interest

All authors declare that they have no known competing financial interests or personal relationships that could have appeared to influence the work reported in this paper.

Disclosures

LLM artificial intelligence agents were used to assist the editing of this manuscript, but all scientific results, concepts, and claims represent original work by the human authors listed.

Data availability statement

The data that support the findings of this study are available from the corresponding author upon reasonable request.

References

[1] A. Fabricant, I. Novikova, G. Bison, How to build a magnetometer with thermal atomic vapor: a tutorial, New Journal of Physics 25 (2) (2023) 025001. doi:10.1088/1367-2630/acb840.

[2] D. Uhland, H. Dillmann, Y. Wang, I. Gerhardt, How to build an optical filter with an atomic vapor cell, New Journal of Physics 25 (12) (2023) 125001. doi:10.1088/1367-2630/ad0fa8.

[3] M. Mäusezahl, F. Munkes, R. Löw, Tutorial on laser locking techniques and the manufacturing of vapor cells for spectroscopy, New Journal of Physics 26 (10) (2024) 105002. doi:10.1088/1367-2630/ad42c6.

[4] P. Tremblay, A. Michaud, M. Levesque, S. Thériault, M. Breton, J. Beaubien, N. Cyr, Absorption profiles of alkali-metal D lines in the presence of a static magnetic field, Physical Review A 42 (5) (1990) 2766–2773. doi:10.1103/PhysRevA.42.2766.

[5] S. Scotto, D. Ciampini, C. Rizzo, E. Arimondo, Four-level N-scheme crossover resonances in Rb saturation spectroscopy in magnetic fields, Physical Review A 92 (6) (2015). doi:10.1103/PhysRevA.92.063810.

[6] H. Stærkind, K. Jensen, J. H. Müller, V. O. Boer, E. S. Polzik, E. T. Petersen, High-field optical cesium magnetometer for magnetic resonance imaging, PRX Quantum 5 (2) (2024) 020320. doi:10.1103/PRXQuantum.5.020320.

[7] S. Scotto, D. Ciampini, R. Battesti, C. Rizzo, E. Arimondo, Rb vapour Zeeman optical spectroscopy in a self-calibrated magnetic field, The European Physical Journal D 80 (1) (2026). doi:10.1140/epjd/s10053-025-01112-9.

[8] R. Momier, A. V. Papoyan, C. Leroy, Sub-doppler spectra of sodium D lines in a wide range of magnetic field: Theoretical study, Journal of Quantitative Spectroscopy and Radiative Transfer 272 (2021) 107780. doi:10.1016/j.jqsrt.2021.107780.

[9] A. Tonoyan, A. Sargsyan, R. Momier, C. Leroy, D. Sarkisyan, Formation of narrow atomic lines of Rb in the uv region using a magnetic field, Optical Memory and Neural Networks 32 (S3) (2023) S343–S348. doi:10.3103/s1060992x23070196.

[10] A. Sargsyan, E. Klinger, A. Amiryan, D. Sarkisyan, Features of alkali D_2 line magnetically-induced transitions excited under π-polarized laser radiation, Physics Letters A 539 (2025) 130372. doi:10.1016/j.physleta.2025.130372.

[11] J. Han, S. Chen, W. Xiao, X. Peng, H. Guo, Optical-beat-frequency measurement of strong magnetic field using a cs micron-thick cell, Physical Review A 111 (3) (2025). doi:10.1103/physreva.111.032813.

[12] Z. Tian, S. Huang, Y. Li, J. Li, S. Ma, Z. Tang, W. Li, Z. Wu, Y. Yang, C. Chen, Y. Zou, Effect of the magnetic-field-induced transition on the intensity ratios of the 3S→ 2P lines in Ne-like ions, Physics Letters A 562 (2025) 131007. doi:10.1016/j.physleta.2025.131007.

[13] A. Tonoyan, A. Sargsyan, E. Klinger, G. Hakhumyan, C. Leroy, M. Auzinsh, A. Papoyan, D. Sarkisyan, Circular dichroism of magnetically induced transitions for D_2 lines of alkali atoms, EPL (Europhysics Letters) 121 (5) (2018) 53001. doi:10.1209/0295-5075/121/53001.

[14] A. Sargsyan, A. Amiryan, A. Tonoyan, E. Klinger, D. Sarkisyan, Coherent optical processes on cs D_2 line magnetically induced transitions, Physics Letters A 434 (2022) 128043. doi:10.1016/j.physleta.2022.128043.

[15] W. D. Williams, M. T. Herd, W. B. Hawkins, Spectroscopic study of the $7p_{1/2}$ and $7p_{3/2}$ states in cesium-133, Laser Physics Letters 15 (9) (2018) 095702. doi:10.1088/1612-202x/aac97e.

[16] M. S. Safronova, U. I. Safronova, C. W. Clark, Magic wavelengths, matrix elements, polarizabilities, and lifetimes of cs, Physical Review A 94 (1) (2016). doi:10.1103/physreva.94.012505.

[17] G. Toh, N. Chalus, A. Burgess, A. Damitz, P. Imany, D. E. Leaird, A. M. Weiner, C. E. Tanner, D. S. Elliott, Measurement of the lifetimes of the $7p^2p_{3/2}$ and $7p^2p_{1/2}$ states of atomic cesium, Physical Review A 100 (5) (2019). doi:10.1103/physreva.100.052507.

[18] A. Sargsyan, R. Momier, D. Sarkisyan, Doppler-free selective reflection spectroscopy of the 6s 7p transition of caesium using an optical nanocell, Journal of Physics B: Atomic, Molecular and Optical Physics 58 (19) (2025) 195001. doi:10.1088/1361-6455/ae0a98.

[19] A. Sargsyan, E. Klinger, R. Boudot, D. Sarkisyan, Doppler-free spectroscopy of the Cs $6S_{1/2} \rightarrow 7P_{3/2}$ atomic transition at 456 nm in a nanometric-thick vapor layer, Optics Letters 50 (10) (2025) 3229. doi:10.1364/ol.558536.

[20] E. Klinger, A. Mursa, C. M. Rivera-Aguilar, R. Vicarini, N. Passilly, R. Boudot, Sub-doppler spectroscopy of the cs atom $6s_{1/2}$–$7p_{1/2}$ transition at 459 nm in a microfabricated vapor cell, Optics Letters 49 (8) (2024) 1953. doi:10.1364/ol.514866.

[21] J. Miao, T. Shi, J. Zhang, J. Chen, Compact 459-nm cs cell optical frequency standard with $2.1 \times 10^{-13}/\sqrt{\tau}$ short-term stability, Physical Review Applied 18 (2) (Aug. 2022). doi:10.1103/physrevapplied.18.024034.

[22] E. Klinger, C. M. Rivera-Aguilar, A. Mursa, Q. A. A. Tanguy, N. Passilly, R. Boudot, Cs microcell optical reference at 459 nm with short-term frequency stability below 2×10^{-13}, Applied Physics Letters 126 (12) (2025). doi:10.1063/5.0261771.

[23] A. Weis, V. A. Sautenkov, T. W. Hänsch, Observation of ground-state Zeeman coherences in the selective reflection from cesium vapor, Physical Review A 45 (11) (1992) 7991–7996. doi:10.1103/physreva.45.7991.

[24] T. A. Vartanyan, D. L. Lin, Enhanced selective reflection from a thin layer of a dilute gaseous medium, Physical Review A 51 (3) (1995) 1959–1964. doi:10.1103/physreva.51.1959.

[25] G. Dutier, S. Saltiel, D. Bloch, M. Ducloy, Revisiting optical spectroscopy in a thin vapor cell: mixing of reflection and transmission as a Fabry–Perot microcavity effect, Journal of the Optical Society of America B 20 (5) (2003) 793. doi:10.1364/josab.20.000793.

[26] H. Failache, S. Saltiel, M. Fichet, D. Bloch, M. Ducloy, Resonant van der Waals repulsion between excited Cs atoms and sapphire surface, Physical Review Letters 83 (26) (1999) 5467–5470. doi:10.1103/physrevlett.83.5467.

[27] A. Laliotis, B.-S. Lu, M. Ducloy, D. Wilkowski, Atom-surface physics: A review, AVS Quantum Science 3 (4) (2021) 043501. doi:10.1116/5.0063701.

[28] V. Sautenkov, S. Saakyan, A. Bobrov, L. Khalutornykh, B. B. Zelener, Spectroscopy of resonantly saturated selective reflection from

high-density rubidium vapor using the pump-probe technique, Journal of Quantitative Spectroscopy and Radiative Transfer 328 (2024) 109153. doi:10.1016/j.jqsrt.2024.109153.

[29] V. Sautenkov, S. Saakyan, A. Bobrov, B. B. Zelener, Optical-field-induced dips and splits in nonlinear spectra of selective reflection from high-density atomic vapor, Journal of Quantitative Spectroscopy and Radiative Transfer 351 (2026) 109796. doi:10.1016/j.jqsrt.2025.109796.

[30] B. A. Olsen, B. Patton, Y.-Y. Jau, W. Happer, Optical pumping and spectroscopy of cs vapor at high magnetic field, Physical Review A 84 (6) (2011). doi:10.1103/physreva.84.063410.

[31] H. Stærkind, K. Jensen, J. H. Müller, V. O. Boer, E. T. Petersen, E. S. Polzik, Precision measurement of the excited state landé g-factor and diamagnetic shift of the cesium d 2 line, Physical Review X 13 (2) (2023) 021036. doi:10.1103/PhysRevX.13.021036.

[32] M. A. Zentile, J. Keaveney, L. Weller, D. J. Whiting, C. S. Adams, I. G. Hughes, Elecsus: A program to calculate the electric susceptibility of an atomic ensemble, Computer Physics Communications 189 (2015) 162–174. doi:10.1016/j.cpc.2014.11.023.

[33] A. Sargsyan, A. Tonoyan, G. Hakhumyan, A. Papoyan, E. Mariotti, D. Sarkisyan, Giant modification of atomic transition probabilities induced by a magnetic field: forbidden transitions become predominant, Laser Phys. Lett. 11 (5) (2014) 055701. doi:doi:10.1088/1612-2011/11/5/055701.

[34] A. Sargsyan, A. Amiryan, E. Klinger, D. Sarkisyan, Features of magnetically-induced atomic transitions of the Rb D_1 line studied by a Doppler-free method based on the second derivative of the absorption spectra, Journal of Physics B: Atomic, Molecular and Optical Physics 53 (18) (2020) 185002. doi:10.1088/1361-6455/ab9f0a.

[35] F. Li, B. Zhao, J. Wei, P. Jin, H. Lu, K. Peng, Continuously tunable single-frequency 455 nm blue laser for high-state excitation transition of cesium, Optics Letters 44 (15) (2019) 3785. doi:10.1364/ol.44.003785.

[36] G. Dutier, A. Yarovitski, S. Saltiel, A. Papoyan, D. Sarkisyan, D. Bloch, M. Ducloy, Collapse and revival of a dicke-type coherent narrowing in a sub-micron thick vapor cell transmission spectroscopy, Europhysics Letters 63 (1) (2003) 35. doi:10.1209/epl/i2003-00474-0.

[37] A. Sargsyan, A. Gogyan, D. Sarkisyan, Features of the van der waals interaction on the cesium $6s_{1/2} \to 7p_{3/2}$ transition in an optical nanocell, Spectrochimica Acta Part B: Atomic Spectroscopy 239 (2026) 107493. doi:https://doi.org/10.1016/j.sab.2026.107493.

[38] C. Andreeva, S. Cartaleva, L. Petrov, S. M. Saltiel, D. Sarkisyan, T. Varzhapetyan, D. Bloch, M. Ducloy, Saturation effects in the sub-Doppler spectroscopy of cesium vapor confined in an extremely thin cell, Physical Review A 76 (1) (2007). doi:10.1103/physreva.76.013837.

[39] F. S. Ponciano-Ojeda, F. D. Logue, I. G. Hughes, Absorption spectroscopy and stokes polarimetry in a ^{87}Rb vapour in the voigt geometry with a 1.5 T external magnetic field, Journal of Physics B: Atomic, Molecular and Optical Physics 54 (1) (2020) 015401. doi:10.1088/1361-6455/abc7ff.

[40] A. Urvoy, Large bandwidth excitation of Rydberg atoms in thermal vapor: Fast dynamics and strong interaction effects, Ph.D. thesis, Dissertation, Stuttgart, Universität Stuttgart, 2016 (2016). doi:10.18419/opus-8852.

[41] J. Liang, T. M. Fuchs, R. Schäfer, V. V. Kresin, Strong permanent magnet gradient deflector for Stern–Gerlach-type experiments on molecular beams, Review of Scientific Instruments 91 (5) (2020). doi:10.1063/5.0007602.